Draft version March 15, 2021
Typeset using LaTeX **modern** style in AASTeX63

Revisit the Oort constants from *Gaia DR2* observations and simulations

Shufan Xia,[1] Karen Masters,[1] and Zhao-Yu Li[2]

[1]*Haverford College, Department of Physics and Astronomy*
[2]*Shanghai Jiaotong University, Department of Astronomy*

1. INTRODUCTION

2. METHODS

2.1. *Theoretic of the Oort constants*

The Oort constants describe stellar streaming motions about the Sun in the Galactic coordinate, a right-handed coordinate where the direction from the Sun to the Milky Way (MW) galactic center is longitude $l = 0$ and positive x. Consider a flat 2D Galactic disk under axisymmetric potential and the cold limit in which all stars move on closed orbits (Olling & Dehnen 2003).The position of a star on the disk is (x,y), where (0,0) is at the Sun in the galactic coordinate. The velocity field $\langle v \rangle$ gives the average velocity at each point on the disk. In solar vicinity, the velocity at (x,y) may be expanded in a Taylor series about the Sun:

$$\langle v \rangle|_{(x,y)} = \langle v \rangle|_{(0,0)} + \begin{pmatrix} v_{xx} & v_{xy} \\ v_{yx} & v_{yy} \end{pmatrix} \Bigg|_{(0,0)} \begin{pmatrix} x \\ y \end{pmatrix} \tag{1}$$

where $\begin{pmatrix} v_{xx} & v_{xy} \\ v_{yx} & v_{yy} \end{pmatrix} = \begin{pmatrix} K+C & A-B \\ A+B & K-C \end{pmatrix} \Bigg|_{(0,0)}$.

The relative velocity of the star as observed from the Sun is given by

$$\delta\langle v \rangle|_{(x,y)} = \langle v \rangle|_{(x,y)} - \langle v \rangle|_{(0,0)} \tag{2}$$

The line of sight velocity is the component of $\delta\langle v \rangle$ parallel to the galactic distance d:

$$v_{los} = \hat{d} \cdot \delta\langle v \rangle = \frac{(x,y)}{d} \cdot \begin{pmatrix} K+C & A-B \\ A+B & K-C \end{pmatrix} \Bigg|_{(0,0)} \begin{pmatrix} x \\ y \end{pmatrix} \tag{3}$$

After taking the dot product and applying trigonometric relations,

$$v_{los} = d[K + A\sin(2l) + C\cos(2l)] \tag{4}$$

Corresponding author: Shufan Xia
sxia1@haverford.edu

Similarly, the longitudinal proper motion, perpendicular component of the relative velocity over d, is:

$$\mu_\perp = \frac{1}{d}(\hat{d} \times \delta\langle v \rangle) = B + A\cos(2l) - C\sin(2l) \tag{5}$$

In the model of local rotation, instead of the actual Sun position because ~~Because~~ the Sun moves in a non-circular orbit about the GC, to account for this non-circular deviation, we define a hypothetical reference point, Local Standard of Rest(LSR), as the origin. The LSR is at the same position of the Sun and moves on a circular orbit 220km s^{-1}, and the relative motions of the Sun with respect to this LSR is described by peculiar motion,(u_0, v_0, w_0), velocity in radial, tangential and vertical direction respectively. After correcting the solar peculiar motion, Eq 4 and 5 turn to:

$$v_{los} = d[K + A\sin(2l) + C\cos(2l)] - u_0\cos(l) - v_0\sin(l) \tag{6}$$

$$\mu_l = B + A\cos(2l) - C\sin(2l) + \frac{1}{d}[u_0\sin(l) - v_0\cos(l)] \tag{7}$$

where the *cosb* term in Eq 7 accounts for the projection of distance onto the Galactic plane in a 3D MW disk. If the vertical velocity v_z of the star is non-zero, the latitudinal relative velocity at (l, b, d) is given by $vz(cosb) - vrsin(b)$ (Olling & Dehnen 2003), and the latitudinal proper motion is:

$$\mu_b = -(Asin2l + Ccos2l + K)sinb\,cosb + \varpi[(u_0 cosl + v_0 sinl)sinb - w_0 cosb] \tag{8}$$

Eq 6, 7 and 8 together give a model to determine Oort constants from observational data, and the full model parameter is $\theta(A, B, C, K, u_0, v_0, w_0)$.

2.2. ~~Selecting Gaia Data~~ Sample selection and stellar parameter estimation.

The Gaia (Global Astrometric Interferometer for Astrophysics) mission of the European Space Agency (ESA) surveys about one billion stars in the MW photometrically and spectroscopically to make the most accurate three-dimensional map of the Galaxy. Gaia samples kinematic tracers dimmer to a magnitude limit of at least $G = 20$ mag in the MW disks, bulge, and halo. The instrument package of Gaia spacecraft comprises two identical optical telescopes/imaging systems, a radial velocity spectrometer, and blue and red photometers. The unfiltered, white-light photometric G band of the optical telescope covers 330–1050 nm (Gaia Collaboration et al. 2016). The parallax uncertainties are 0.5 mas at $G = 20$. The uncertainties in proper motion are 0.5 mas yr^{-1} at $G = 20$ (Gaia Collaboration et al. 2018).

The radial-velocity spectrometer obtains radial velocities by measuring the Doppler-shift in the lines of stellar spectra. DR2 has the radial velocity of more than 7.2 million stars with a mean $G = 4 - 13$ mag and an effective temperature in the range 3550 to 6900 K. The overall precision of the radial velocities range from 200-300 m s^{-1} to 1.2-3.5 km s^{-1}(Gaia Collaboration et al. 2016).

Astrophysical parameters such as effective temperature, surface gravity, metallicity, and extinction are derived from the BP/RP data measured by the blue and red photometers over the wavelength ranges 330–680 nm and 630–1050 nm (Gaia Collaboration et al. 2016).

In December 2020, ESA released the third intermediate *Gaia* data (EDR3). This version of release catalogs the positions and proper motions, and other photometric data of 1,811,709,771 stars, 1,692,919,135 entries of which are updated from DR2. The radial velocity data in EDR3 is added from the 7.2 million data in DR2 after deleting 4000 wrong entries. Furthermore, EDR3 deleted several entries from DR2, including color excess, extinction, and tag for marking variable star samples (Gaia Collaboration et al. 2020). I used the TAP service from TOPCAT (Tool for Operations on Catalogues And Tables) to access, process, and select the DR2 and EDR3 data (Taylor 2005).

Since the first-order Taylor approximation is only appropriate for solar vicinity, the stellar samples are limited to the region within 500 pc (2mas) from the sun. And restricting parallax/error$\geq$ 10 will avoid additional bias from inverting the parallax to estimate distance (Luri et al. 2018). The uncertainties in the BP and RP fluxes are restrained to less than 10% in making an HR diagram and selecting the main sequence samples. Potential duplicate sources are also removed.

The main sequence stars are selected by drawing on the H-R diagram in TOPCAT. Extinction A_G and color excess $E(B-V)$ must be considered when making an H-R diagram to reflect the properties of stars accurately. However, spectroscopic data, such as radio velocity, extinction, and color excess are not yet available for the 100 million newly added stars in EDR3. These data are expected to be published in DR3 in the first half of 2022 (Gaia Collaboration et al. 2020). Instead of doing a cross-match with DR2 samples, $E(B-V)$ in EDR3 are calculated from the DUSTMAP python library because the new spectroscopic measurements in EDR3 and DR3 use different blue and red photometers than those in DR2. DUSTMAP gives a 3D map of interstellar dust reddening probabilistically based on broadband photometric measurement from Pan-STARRS 1, 2MASS, and Gaia parallaxes (Green 2018). Each (l, b, d) corresponds to a color excess value in the default *bayestar17* module in DUSTMAP, which I multiplied with $R_v = 3.1$ to get the extinction. For EDR3, the position data is first retrieved from TOPCAT, then used to find $E(B-V)$ and A_G in python. The original data along with calculated $E(B-V)$ and A_G are used to plot H-R in TOPCAT again, and I drew out the main sequence samples on this diagram. Fig 1 shows the H-R diagram and Main sequence star samples in DR2 and EDR3 after applying parallax, extinction and color excess corrections. For DR2, color excess and extinction values used are from Gaia observation.

~~2.3. *Calculating the Oort Constants*~~ (This section can be merged with the previous one)

* It is better to merge the two plots together with the same x y axis range and axis ratio, use hist 2d to show this kind of figure.

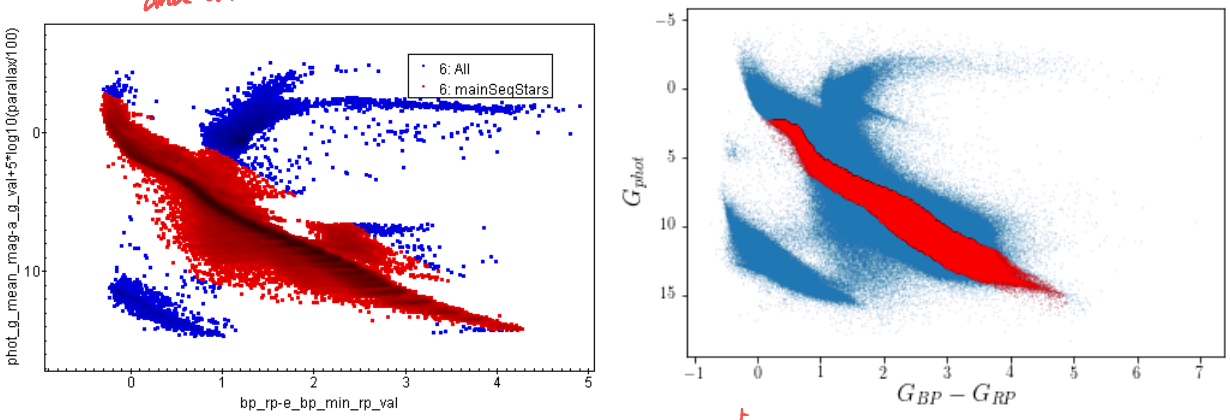

(a) H-R diagram for DR2 (b) DR3 (corrected plot not available yet)

Figure 1: the H-R diagram and Main sequence star samples in DR2 and EDR3 after parallax, extinction and color excess correction.

Because the local Oort constants varied among different stellar populations based on their color, thus their collective kinematic properties, I grouped the main sequence stars into six color groups on the H-R diagram based on color according to the criteria of Li et al. 2019. The rotational kinematics properties and the corresponding Oort constants for color group are analyzed individually. Table1 shows the number of stars in each stellar group, as well as the corresponding numbers in DR2.

$BP\_RP - e\_bp\_min\_rp\_val$	< 0.8	$0.8- < 1.2$	$1.2 - 1.6$	$1.6- < 2.0$	$2.0 - 2.4$	≥ 2.4
DR2	448141	708555	560939	438289	143526	127939
EDR3	649939	792940	1304201	2173292	347488	9356

Table 1: Number of main sequence stars fall into each color group for DR2 and EDR3. (will update these counts)

The proper motions and radial velocity entries in Gaia are measured in the equatorial coordinates system (ICRS), i.e. right ascension (α) and declination (δ) proper motions, μ_α and μ_δ. I used the SkyCoord class in *astropy*(Astropy Collaboration et al. 2018) to transform proper motions and available radial velocity from ICRS to the Galactic coordinate. The units of proper motion are also converted from mas yr^{-1} to km s^{-1} kpc^{-1} by multiplying 4.74047. The uncertainties of proper motions are obtained via error propagation from equatorial coordinates. The equations for equatorial coordinates transformation derived are given by Poleski 2013:

$$\mu_l = \frac{1}{cosb}(C_1\mu_\alpha + C_2\mu_\delta), \tag{9}$$

$$\mu_b = \frac{1}{cosb}(-C_2\mu_\alpha + C_1\mu_\delta) \tag{10}$$

where

$$C_1 = sin\delta_G cos\delta - cos\delta_G sin\delta cos(\alpha - \alpha_G),$$
$$C_2 = cos\delta_G sin(\alpha - \alpha_G)$$
$$cosb = \sqrt{{C_1}^2 + {C_2}^2} \text{ and } \alpha_G = 192°.86, \delta_G = 27°.13.$$

Applying the partial derivative rules in error propagation, I found the error in proper motions after coordinate transformation:

$$\sigma^2_{\mu_l} = \sigma^2_b(\frac{\partial \mu_l}{\partial b})^2 + \sigma^2_\alpha(\frac{\partial \mu_l}{\partial \alpha})^2 + \sigma^2_\delta(\frac{\partial \mu_l}{\partial \delta})^2 + \sigma^2_{\mu_\alpha}(\frac{\partial \mu_l}{\partial \mu_\alpha})^2 + \sigma^2_{\mu_\delta}(\frac{\partial \mu_l}{\partial \mu_\delta})^2 \tag{11}$$

and the corresponding errors

2.4. *Estimating the parameters ~~uncertainties~~: Monte-Carlo-Markov-Chain (MCMC)*

The parameters in the model of Eq 6, 7 and 8 consist of the four Oort constants and three peculiar velocity components. For such high-dimensional parameter space, I used the Monte Carlo Markov Chain method to determine the value and uncertainty of each parameter. The MCMC method combines our prior knowledge about the model and evidence from the data to obtain a posterior distribution of the model parameter θ, in this case, $\theta(A, B, C, K, u0, v0, w0)$. When fitting Gaia observational data in MCMC, the proper motions in longitude and latitude direction are considered together, but radial velocity is separated because this data is incomplete. The logarithmic likelihood function used is defined as:

*You can dig a little deeper to explain the concept of Monte-Carlo simulation and Markov-chain, and how these methods can help us to find the error of the best-fit parameters

$$ln\mathcal{L}_\infty = -\sum_i \left(\frac{(med(\mu_l)_i - {y_1}_i^2}{\sigma^2_{med(\mu_l)} + error^2_{med(\mu_l)}} - ln\frac{2\pi}{\sigma^2_{med(\mu_l)} + error^2_{med(\mu_l)}} \right.$$
$$\left. + \frac{(med(\mu_b)_i - {y_2}_i^2}{\sigma^2_{med(\mu_b)} + error^2_{med(\mu_b)}} - ln\frac{2\pi}{\sigma^2_{med(\mu_b)} + error^2_{med(\mu_b)}} \right) \tag{12}$$

where $\sigma_{med(\mu_l)}$ and $\sigma_{med(\mu_b)}$ are the Gaussian scatter for the distribution of binned medians, $error^2_{med(\mu_l)}$ and $error^2_{med(\mu_b)}$ are the standard deviations within each bin, and y_1 and y_2 are given by Eq 7 and 8.

The prior distribution of θ is defined as following:

$$P(\theta) = \begin{cases} 0 & \text{if } 10 < A < 20, \ -15 < B < -5\ , -5 < C < 5, \text{ and } -5 < K < 5 \\ -\infty & \text{if A, B, C and K are not within the range above} \end{cases} \tag{13}$$

And the overall logarithmic posterior probability is:

$$LnP(\theta|y) = \begin{cases} lnL & \text{if } P(\theta) = 0 \\ 0 & \text{if } P(\theta) = -\infty \end{cases} \tag{14}$$

I employed the *emcee* (Foreman-Mackey et al. 2013) python package and posterior probability Eq 14 to sample and update Markov Chains in MCMC.

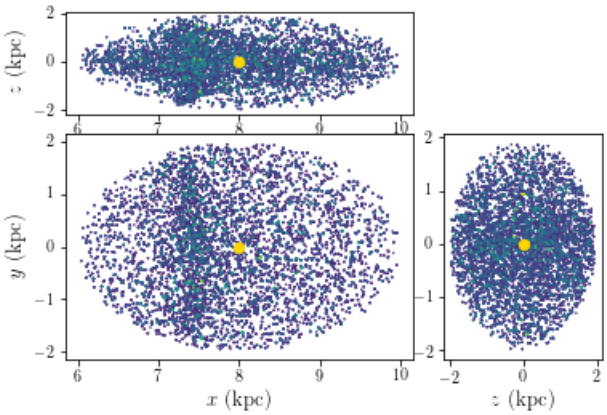

Figure 2: the spatial distribution of test particles within 2kpc from the Sun based on the quasi-isothermal distribution

2.5. *Simulation*

To know what behaviors are expected from the theoretical Oort constants model, and thus understand how the actual MW deviates from the theoretical model, I did a toy model simulation, treating stars as test particles and assuming all the model constraints of the Oort constants and the Sun stays on a circular orbit. I sampled 20,000 of test particles from *galpy*'s quasi-isothermal distribution function to represent a thin 3D Milky Way galactic disk. The distance from the Sun to the Galactic center and the circular velocity at the solar radius are set to $R_0 = 8$ kpc and $v_0 = 220$ km/s. This distribution function provides planar and vertical profiles of the thin disc with analytic function dependent on the action integrals in an integrable, axisymmetric Hamiltonian (Binney 2010). The potential in the Hamiltonian is specified by MWPotential2014.

MWPotential2014 serves as a simple and accurate model for the MW potential from fitting to a large variety of dynamical data. This potential model consists of a bulge potential with a power law exponent of 1.8 and a cut-off radius of 1.9kpc (PowerSphericalPotentialwCutoff), a disk potential specified by MiyamotoNagaiPotential, and a dark-matter halo described by an NFWPotential (Bovy 2015). Fig 2 shows the spatial distribution of test particles within 2kpc from the Sun sampled from the quasi-isothermal distribution function.

All particles undergo 10Gyr of orbit integration under the potential specified by MWPotential2014 to reach equilibrium. The positions and velocities after 10Gyr are then used to calculate μ_l and μ_b, as well as v_{los}. Similar the procedure of analyzing Gaia data, I binned the simulation data and used the binned medians to fit the three equations in Eq 6, 7 and 8, except u0, v0, and w0 are set to 0. The log likelihood for MCMC is defined as:

$$ln\mathcal{L}_2 = ln\mathcal{L}_1 - \sum_i \left(\frac{(med(v_{los})_i - y_{3_i}^2}{\sigma^2_{med(v_{los})} + error^2_{med(v_{los})}} - ln \frac{2\pi}{\sigma^2_{med(v_{los})} + error^2_{med(v_{los})}} \right) \quad (15)$$

where $ln\mathcal{L}_1$ is from Eq 12, $\sigma_{med(v_{los})}$ is the Gaussian scatter for the distribution of binned medians of v_{los}, $error_{med(v_{los})}$ is the standard deviations within each bin of v_{los}, and y_3 is given by Eq 6.

REFERENCES

Astropy Collaboration, Price-Whelan, A. M., SipHocz, B. M., et al. 2018, aj, 156, 123, doi: 10.3847/1538-3881/aabc4f

Binney, J. 2010, MNRAS, 401, 2318, doi: 10.1111/j.1365-2966.2009.15845.x

Bovy, J. 2015, ApJS, 216, 29, doi: 10.1088/0067-0049/216/2/29

Foreman-Mackey, D., Hogg, D. W., Lang, D., & Goodman, J. 2013, PASP, 125, 306, doi: 10.1086/670067

Gaia Collaboration, Brown, A. G. A., Vallenari, A., et al. 2020, arXiv e-prints, arXiv:2012.01533. https://arxiv.org/abs/2012.01533

Gaia Collaboration, Prusti, T., de Bruijne, J. H. J., et al. 2016, A&A, 595, A1, doi: 10.1051/0004-6361/201629272

Gaia Collaboration, Brown, A. G. A., Vallenari, A., et al. 2018, A&A, 616, A1, doi: 10.1051/0004-6361/201833051

Green, G. 2018, The Journal of Open Source Software, 3, 695, doi: 10.21105/joss.00695

Li, C., Zhao, G., & Yang, C. 2019, ApJ, 872, 205, doi: 10.3847/1538-4357/ab0104

Luri, X., Brown, A. G. A., Sarro, L. M., et al. 2018, A&A, 616, A9, doi: 10.1051/0004-6361/201832964

Olling, R. P., & Dehnen, W. 2003, ApJ, 599, 275, doi: 10.1086/379278

Poleski, R. 2013, arXiv e-prints, arXiv:1306.2945. https://arxiv.org/abs/1306.2945

Taylor, M. B. 2005, in Astronomical Society of the Pacific Conference Series, Vol. 347, Astronomical Data Analysis Software and Systems XIV, ed. P. Shopbell, M. Britton, & R. Ebert, 29